Theoretical tools and concepts for modelling growing plant tissues

Oliver E. Jensen
School of Mathematics, University of Manchester, UK *

July 14, 2019

In these lectures[1] I will review some of the approaches taken to model the mechanical properties of growing plant tissues. I will start in §1 by discussing the contrasting nature of stress and strain in multicellular tissues undergoing so-called *diffuse* growth. (I will not discuss tip growth of pollen tubes or root hairs, nor secondary growth of lignified tissues.) I will then (§2) review simple constitutive laws in one spatial dimension (1D) and introduce the widely used Lockhart model for cell and tissue expansion. I will show how to convert a discrete (cell-scale) model into a continuous (tissue-scale) model (§3) and explain how 1D constitutive models can be used to model 2D bending (§4), using root gravitropism as an example. In §5, I will describe how the Lockhart model can be formulated in 3D for continuous materials, accounting for anisotropy and growth, as is used in current computational studies. I will then turn to computational models for individual cells (§6), focusing on the widely-used *vertex-based* framework where cells are described as polygons or polyhedra. This is a popular framework in developmental biology and offers an interesting contrast to traditional continuum models. Finally, I will review some models of the plant cell wall (§7), examining its fundamental role in shaping organisms.

I will assume familiarity with basic continuum mechanics and make some use of vector and tensor calculus and a little linear algebra. More mathematical material appears in boxes; results are summarised outside them. Technical terms are presented in italics when they are first introduced. There is not space here to be fully comprehensive and the topics presented are deliberately selective, influenced by my own experience working on root growth [37]. An excellent resource giving a wider view of mechanical modelling of growing tissues is [31]. Other more plant-specific reviews include [1, 40, 43, 56].

1 An introduction to the mechanics of multicellular materials

Deformations of plant tissues may be passive (a stem bending in the wind or a leaf or hanging under gravity) or active (involving growth, through cell division and cell elongation). Setting aside cell division for the time being, let us consider the implications of the observation that plant cells generally remain tightly adhered to their neighbours (in so-called *symplastic growth*). In the absence of dramatic deformations that lead to fracture, strains must then be reasonably smooth functions of position, varying slowly from cell to cell in a tissue. This does not preclude the plant from undergoing large deformations, as small strain gradients can accumulate along slender structures to allow substantial deformations. This is of critical importance in allowing a plant to accommodate and exploit its environment. For example, differential expansion drives the bending of a gravitropic root [44] or the unfurling of an anther [47]. Likewise a long slender leaf can be strongly deformed in a breeze [20] without the strains on its tissues being large enough to cause irreversible deformations.

Plant cells are heterogeneous structures, with soft pressurized interiors and relatively stiff cell walls. While deformations may generally be smoothly varying functions of position, the resulting stress fields may not be. In particular, stress in a biological material can be very sensitive to the size and location of the domain over which it is measured (see box below). This raises interesting questions about the distribution of stress within a cell, and how stress (or strain) is sensed within a cell. Cosgrove [17] discusses some of the challenges of measuring material properties of plant tissues at small scales.

*Oliver.Jensen@manchester.ac.uk
[1]Delivered at the 24th CISM-IUTAM International Summer School on Plant Biomechanics, Udine, Italy, July 8-12 2019

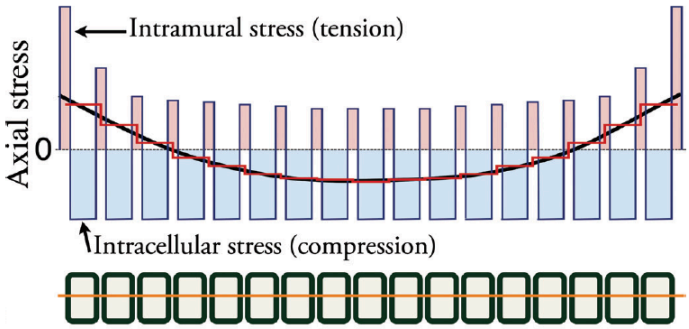

Figure 1: The blue line (top) illustrates the axial component of stress in a layer of cells (green, below) lying across the cross-section of a stem. Stress is sampled along the orange line that intersects cell walls and cytoplasm (treated as vacuoles), with walls under tension and vacuoles under compression. The stress field therefore fluctuates from positive (pink) to negative (blue) values with respect to a reference level. Averaging the stress across each cell (red line) indicates how cells in the centre of the stem may be under net compression, while those near the periphery may be under net tension. The black curve shows the smoothly varying stress field when it is averaged over multiple cells. When averaged over the whole stem, the stress field may vanish (dotted line), even though individual components of the tissue may be subject to large tensile or compressive stresses. From [5].

The (Cauchy) stress $\boldsymbol{\sigma}$ of a material can be interpreted with respect to a sample area A with unit normal $\hat{\mathbf{n}}$, such that the force exerted on A is $\int_A \boldsymbol{\sigma}\cdot\hat{\mathbf{n}}\,\mathrm{d}A$. (That is to say, on each small element $\mathrm{d}A$ of the surface A, the tensor $\boldsymbol{\sigma}$ maps the vector $\hat{\mathbf{n}}$ to a new vector (a stress) $\boldsymbol{\sigma}\cdot\hat{\mathbf{n}}$, leading to a force $\boldsymbol{\sigma}\cdot\hat{\mathbf{n}}\,\mathrm{d}A$. The total force on A is an integral (a sum) over all such elements.) If $\hat{\mathbf{n}}$ is uniform over A, we may therefore define the *average stress* over the sample area $\langle\boldsymbol{\sigma}\rangle \equiv (1/A)\int\boldsymbol{\sigma}\,\mathrm{d}A$. For a material with microstructure, we expect the average stress to be well defined (i.e. to have a robust statistical average) for sufficiently large A. However $\langle\boldsymbol{\sigma}\rangle$ is likely to be highly variable for small A, depending on which component of the microstructure is being sampled.

Consider for example a primary root or stem, shown as a cartoon in Fig. 1. Each cell contains a vacuole that draws in water from its environment, generating a high osmotic pressure (of approximate magnitude RTC, where $R \approx 8.3\mathrm{JK}^{-1}\mathrm{mol}^{-1}$ is the ideal gas constant, T the absolute temperature and C the solute concentration in the vacuole). The tendency of the cell to inflate is restricted by the stiff cell wall, generating a tension in the cell wall. The balance between expansive forces in the cytoplasm, and tensile forces in the cell periphery, give the cell an intrinsic rigidity (like an inflated balloon). Strong adhesion forces between neighbouring cells reinforce this effect, rigidifying the tissue. (I will not here discuss secondary mechanisms of stiffening through deposit of woody material.) Across a cross-section of a stem, therefore, we expect to see alternating regions of tensile and compressive tissue (Fig. 1). When measured with respect to sufficiently small areas A, the stress field fluctuates dramatically across individual cells. However, once integrated over multiple cells, we can consider a field that varies more smoothly. Fig. 1 illustrates a postulated stress field whereby cells at the periphery of the stem are under net tension, while those nearer the centre are under net compression (mimicking the stress field within individual cells), even though the stress averaged across the whole stem cross-section may vanish. This particular distribution of so-called 'residual stress' helps give the stem rigidity [59]. (Similarly, the shoot apical meristem has a stiff epidermal layer, which can be modelled as a pressurized shell [8, 39].) Stress is hard to measure non-invasively but reveals itself when the stem is cut, allowing central cells to elongate, peripheral cells to shrink, causing the cross section to bulge (try this with an onion!).

The stress field in Fig. 1 illustrates the mathematical idea of *homogenization*, whereby a fluctuating field is approximated by its spatial average, which may vary smoothly over long lengthscales. For plant tissues, we might wish to treat the tissue as a continuum (smoothing out the variations over individual cells) and seek a mechanical model formulated in terms of partial differential equations (PDEs) relating the slowly-varying stress field to strain or strain rate, to model deformation under loading or growth. A *constitutive assumption* is required, capturing the mechanical properties of the tissue (as linearly or nonlinearly elastic, viscoelastic, etc.) and possibly including a framework for modelling growth (e.g. the popular Skalak–Rodriguez formulation [52, 54]). I will review a set of such models below, starting from simple spatially 1D descriptions (very useful for slender structures) before moving to 3D.

A key question in this approach is to define the appropriate constitutive model. One then asks: how are the macroscopic parameters describing a tissue related to the geometric and physical properties of its microstructure? This question motivates models that resolve individual cells, or components within them. In principle, a cell-scale model can be carefully averaged to derive bulk tissue properties. When cells have a highly organised arrangement (for example a periodic lattice), then the averaging can be performed systematically (via *asymptotic* or *two-scale* homogenization). More generally, however, there will be a degree of spatial disorder in the tissue, which raises interesting questions about the validity of averaging procedures. The inherently discrete nature of a multicellular tissue may even present mechanical features (such as *force chains* [26]) that are lost via spatial averaging.

Even in *upscaling* from cells to tissues, a constitutive assumption is needed to describe cell properties, which in turn raises questions about cell microstructure. For plant cells, attention turns immediately to the cell wall, a composite material in which stiff cross-linked cellulose fibres are embedded in a pectin matrix. Plant cells regulate the material properties of the wall, and in particular the orientation of the fibres within it, to influence cell, tissue and organ properties. Key concepts here are *anisotropy* (material properties that vary with orientation with respect to the fibre distribution) and *plasticity* (irreversible deformations that arise for materials that are subject to sufficiently large stress or strain). Plants present a fascinating challenge in that the molecular microstructure (fibre orientation in cell walls, at the sub-micron scale) can influence organ shape (up to metre scales). Alongside the 'bottom-up' question of how microstructure influences macroscopic properties, we must also consider the 'top-down' question of how the plant senses its environment (via signals associated with gravity, light, water, nutrients, etc.) and responds at the molecular level. Hierarchies of mathematical and computational models are needed that can efficiently communicate information up and down scales (exemplifying the challenge of *multiscale modelling*).

This endeavour is complemented by the increasing availability of 3D imaging of plant tissues, allowing detailed geometric data to be integrated with models of mechanical and biological function. To some extent this is beguiling: while shape (and the distribution of specific molecules) can be studied in exquisite detail, measurement of mechanical properties and particularly of stress (as mentioned above) remains much more challenging. Theoretical and computational models are essential in inferring mechanical properties from imaging data and stress assays.

2 Simple constitutive models and Lockhart's equation

We have already briefly encountered Cauchy stress $\boldsymbol{\sigma}$. In nonlinear elasticity, different representations of stress can be used, defined with respect to the deformed or underformed configurations of a material. For small deformations, however, these distinctions can be ignored, and for slender structures it is often sufficient to focus on a single dominant (axial, scalar) component σ, with dimensions force/area. When integrated over the thickness of structure, the resulting force is sometimes called a *stress resultant* (dimensions force/length).

Likewise, large deformations of materials in 3D need careful definition of strain. For small (axial) deformations of slender structures, however, it is sufficient to represent the strain as the *relative elongation* $e = \delta l/l$ for an object of length l deforming by extension δl. When length $l(t)$ varies with respect to time t, the *strain rate* $\dot{e} = (1/l)\mathrm{d}l/\mathrm{d}t$, is termed the *relative elongation rate* (RER) or *relative elementary growth rate* (REGR) in the plant science community and is a central quantity in modelling growth by elongation.

We now revisit some standard constitutive descriptions of materials, moving towards the *elasto-viscoplastic*

model that is commonly used to model growing plant tissues. Cosgrove [18] makes the important point about accuracy in terminology: wall 'softness' for example is vague, as it does not distinguish between *compliance* (an elastic property) from *extensibility* (a viscous property).

2.1 Simple constitutive laws in one dimension

For an **elastic** material, deformation is fully reversible: a load induces a strain and removal of the load causes the material to recover its initial state. At a molecular level, it is assumed there is no breakage of molecular bonds. In 1D, we write $\sigma = Ee$ for some stiffness E (associated with the Young's modulus). This linear relation is a statement of Robert Hooke's famous 'law.' There is an associated *strain energy* $W = \frac{1}{2}Ee^2$, so that $\sigma = \mathrm{d}W/\mathrm{d}e$ and $E = \mathrm{d}^2W/\mathrm{d}e^2$.

For a **viscous** material, deformation is irreversible (implying breakage of molecular bonds), and the material does not return to its original configuration after a load is removed. In 1D, we write $\sigma = \mu\dot{e}$ for some viscosity μ, where a dot denotes a time derivative. This can be inverted to read $\dot{e} = \phi\sigma$ where $\phi = \mu^{-1}$ is called an *extensibility* in the plant science community. $\sigma\dot{e} = \mu\dot{e}^2$ is the rate at which energy is dissipated by bond breakage.

For **viscoelastic** materials, two basic formulations are normally adopted, with viscous and elastic elements assumed to act in series (Maxwell) or in parallel (Kelvin), representing predominantly fluid-like or solid-like materials respectively. When in parallel (so that the stresses of each element contribute to the total stress), we write $\sigma = Ee + \mu\dot{e}$. When in series (so that the strains of each element contribute to the total strain), we write

$$\dot{e} = \phi\sigma + E^{-1}\dot{\sigma}. \tag{2.1}$$

These expressions reveal a *relaxation time* $\mu/E \equiv E^{-1}/\phi$ over which the material responds to a change in loading conditions. For example the Maxwell model describes how, under a step-change in deformation, there is a rapid elastic response, followed by *relaxation* of the stress to zero. Alternatively the Kelvin model describes *creep*, the time-dependent deformation arising in response to a step-change in stress. More elaborate combinations of elements can be used to model more complex responses.

To describe a **plastic** material we must introduce the concept of a *yield stress* Y (or possibly a *yield strain*), below which the material remains (largely) undeformed but above which there is irreversible deformation. The viscous model is adapted to read

$$\dot{e} = \phi(\sigma - Y)_+ \tag{2.2}$$

where the + subscript denotes (for a scalar argument) a *Heaviside function*: $(x)_+ = x$ if $x > 0$ and $(x)_+ = 0$ otherwise. This innocuous constitutive law (2.2) (sometimes called a *Bingham model*) is piecewise linear but the discontinuity makes it strongly nonlinear (not even everywhere differentiable). Yield is a complex topic, reviewed in [11].

We can combine (2.1, 2.2) to form a (Maxwell) **elasto-viscoplastic** material, satisfying

$$\dot{e} = \phi(\sigma - Y)_+ + E^{-1}\dot{\sigma}. \tag{2.3}$$

Weak loads, for which σ remains below Y, lead to reversible elastic deformation with $\sigma = Ee$. Stronger loads irreversibly deform the material. This model can be used to explain the way in which a ribbon (or a strip of paper) can be curled by running it over a blade, provided it is under sufficient load [51].

In an equivalent formulation, one can write $e = e_e + e_g$, decomposing the strain in adjacent Maxwell elements into that due to the elastic component $e_e = \sigma/E$, and that arising from plastic deformation (which will be used to mimic growth). Let $e_Y = Y/E$ be the yield strain associated with the yield stress. Then (2.3) can be re-expressed as

$$e_e = E^{-1}\sigma, \quad \dot{e}_g = \phi E(e_e - e_Y)_+, \quad e = e_e + e_g, \tag{2.4}$$

so that a load σ induces an (internal) elastic strain which, if large enough, increases the unloaded length of the material. This formulation turns out to be useful when moving to higher dimensions [12].

It is important to remember that all of these constitutive models are based on very restrictive assumptions. A real material is likely to have complex behaviour that falls outside these standard descriptions. Obvious missing features are dimensionality (considering 2D or 3D rather than 1D deformations, so involving additional components of stress and strain), nonlinearity, anisotropy, heterogeneity and, for plants, active processes that lead to growth.

2.2 Lockhart's model

Lockhart [41] introduced an influential model for the expansion of a single plant cell. Suppose that an isolated thin-walled cylindrical cell elongates along its axis. Its volume is $V = Al$, where A is its cross-section. As long as A is constant, then the volumetric strain rate is equivalent to the linear strain rate,

$$\frac{1}{V}\frac{\mathrm{d}V}{\mathrm{d}t} = \frac{1}{l}\frac{\mathrm{d}l}{\mathrm{d}t} = \dot{e}. \tag{2.5}$$

If P is the pressure within the cylinder, then a force balance on the end plate (assuming the cell is under no external load) gives

$$PA = Tp \tag{2.6}$$

where T is the axial stress resultant (axial tension) in the cell wall and p the perimeter. (For a circular cross section, $A = \pi R^2$ and $p = 2\pi R$ where R is the cell radius, so that $T = PR/2$.) If we adopt a 1D viscoplastic model for the cell wall (2.2), then

$$\frac{1}{l}\frac{\mathrm{d}l}{\mathrm{d}t} = \phi(\sigma - Y)_+ \tag{2.7}$$

where $\sigma = T/h$ and Y is a yield stress. (We integrate σ over the wall thickness h to obtain T.) Then (2.5) and (2.6) give

$$\frac{1}{V}\frac{\mathrm{d}V}{\mathrm{d}t} = \theta\phi\left(P - \frac{Y}{\theta}\right)_+ \quad \text{where} \quad \theta \equiv \frac{A}{ph}. \tag{2.8}$$

The geometric structure of the cell, captured through the dimensionless ratio θ, converts the wall extensibility ϕ and wall yield stress Y to an effective cell extensibility $\theta\phi$ and cell yield stress Y/θ. We will shortly see how the viscoplastic structure of the model is preserved as we move up to tissue level.

> The axial stress resultant in an inflated circular cylindrical cell is $T = PR/2$. Away from the ends of the cell, there is an additional transverse (or hoop) stress resultant in the curved cell wall, given by the *Young–Laplace* condition as PR, exactly double the axial stress. This is a simple feature of an engineering *pressure vessel*.

A plant cell regulates its turgor pressure using salts that draw in water from its surroundings by osmosis. The flux per unit area across the wall is given by a *Starling relation*, of the form $J = k(\Delta P - \Delta\Pi)$, where ΔP is a hydrostatic pressure difference and $\Delta\Pi$ an osmotic pressure difference. k is a *permeability*. For simplicity, let us assume that the hydrostatic and osmotic pressures are zero outside the cell, and that the flux takes place across the curved wall of the cell, of area pl. Then mass conservations demands that

$$\frac{\mathrm{d}V}{\mathrm{d}t} = plk(\Pi - P). \tag{2.9}$$

If we assume that P is large enough to allow cell expansion, we can eliminate P between (2.8) and (2.9) to obtain

$$\frac{1}{V}\frac{\mathrm{d}V}{\mathrm{d}t} = \frac{\phi\theta\,[\Pi - Y/\theta]}{1 + (\phi\theta^2 h/k)} \tag{2.10}$$

if $\Pi - Y/\theta$ is sufficiently large. The parameter $\phi\theta^2 h/k$ represents a ratio of the time taken for water to cross the cell wall to the time taken for the cell to elongate. If water transport is rapid, which is a conventional assumption, then $\phi\theta^2 h/k \ll 1$, $P \approx \Pi$ and

$$\frac{1}{l}\frac{\mathrm{d}l}{\mathrm{d}t} = \phi\theta\,[\Pi - Y/\theta]_+\,. \tag{2.11}$$

This demonstrates how the cell acts as an osmotic pump. Provided salts can be concentrated sufficiently (increasing the osmotic pressure Π), then water is drawn quickly into the cell, increasing its volume. Lockhart's model treats growth as a visco-plastic process, with molecular bonds being broken irreversibly in the cell wall to allow its elongation. The assumption that the wall thickness h remains constant as the cell elongates implicitly accounts for active metabolic processes that deliver new material to the cell wall (which would be expected to thin as it stretches), allowing the wall to maintain its thickness as it expands. The coupling between water fluxes and growth is examined in [15].

Finally, in some circumstances it is helpful to incorporate the elastic response of the cell as well, in which case (2.3) leads to

$$\frac{1}{l}\frac{\mathrm{d}l}{\mathrm{d}t} = \phi\theta\left[\Pi - Y/\theta\right]_+ + \theta E^{-1}\frac{\mathrm{d}\Pi}{\mathrm{d}t}. \tag{2.12}$$

Equivalently, following (2.4),

$$e_e = \Pi\theta/E, \quad \dot{e}_g = \phi E\left[e_e - e_Y\right]_+, \quad e = e_e + e_g, \tag{2.13}$$

where the yield strain is $e_Y = Y/E$. If one introduces $\bar{l}$ as the length the cell would take due to growth alone, a variation of this model has

$$e_e = \Pi\theta/E, \quad \dot{\bar{l}}/\bar{l} = \phi E\left[e_e - e_Y\right]_+, \quad l = e_e\bar{l}. \tag{2.14}$$

We will see later how this model is formulated in 3D.

3 One-dimensional models for elongation of slender tissues

Roots and shoots can be long and slender, encouraging the use of a spatially 1D description. Let's consider how to model a line of elongating cells, moving from a discrete description of individual cells formulated as sets of ODEs to a continuous description formulated using PDEs. An early treatment of this problem was given by [53].

3.1 A continuous model for primary root growth

A primary root has a meristem at its tip, in which cell division and differentiation take place. Immediately behind the meristem is an *elongation zone* (EZ), in which tightly adherent cells lengthen rapidly before maturing. In this simple treatment, we will assume no cell division takes place in the EZ. In the frame of reference of the root tip, there is a flux of cells through the EZ in the shootwards direction, leaving the EZ at some speed v_∞. Mature cells are stationary with respect to the plant and its environment, implying that in this frame of reference the elongation zone and meristem propagate downwards through soil at speed v_∞.

Let x measure distance along a line of root cells, measured from the meristem. We suppose cells are introduced at $x = 0$ through a process of cell division. Let cell j occupy $X_{j+1}(t) < x < X_j(t)$, so that it has length $L_j = X_j - X_{j+1}$. Its speed with respect to the meristem is $V_j = \frac{1}{2}(\dot{X}_j + \dot{X}_{j+1})$. (It is convenient to label cells entering the tissue with increasing values of j.) We assume each cell undergoes elongation according to a Lockhart law before maturing at the downstream end of an elongation zone. If cells enter the domain with fixed period c, then the tissue will appear stationary when viewed through a stroboscope with the same period, i.e. $X_j(t) = X_{j+1}(t + c)$, as illustrated in Fig. 2.

The trajectories of cell vertices are shown in a space-time plot in Fig. 3. Horizontal distances between the curves show increasing cell lengths. The slope of each curve diminishes with respect to x, reflecting increasing speed with respect to the meristem. To understand how spatial observations reveal the time-evolution of individual cells, we approximate the discrete model for individual cells as a continuous model for a tissue.

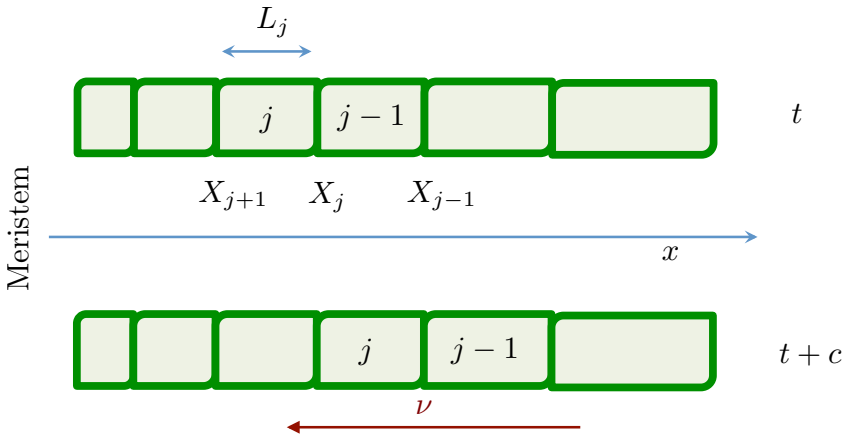

Figure 2: Cells at time t (top) and at time $t+c$ (bottom), where c is the division time over which a new cell enters the domain, in the frame of reference of the meristem (left) from which the cells emerge. Mature elongated cells exit the domain at the right. x measures distance from the meristem; ν is a variable counting (and anchored to) cells, increasing in the opposite direction.

If the cell length and speed vary sufficiently smoothly with respect to j, we can imagine interpolating the discrete functions L_j and V_j with smooth analogues $l(\nu,t)$ and $v(\nu,t)$, where ν is a *Lagrangian* variable such that $l(j,t) = L_j(t)$ and $v(j,t) = V_j(t)$. The location of cell vertices is $x(j,t) = X_j(t)$. Approximating differences with derivatives, so that

$$\left.\frac{\partial x}{\partial \nu}\right|_t \approx X_{j+1} - X_j, \quad c\left.\frac{\partial x}{\partial t}\right|_\nu \approx X_j(t+c) - X_j(t), \tag{3.1}$$

we have (to leading order)

$$l = -\frac{\partial x}{\partial \nu}, \quad v = \frac{\partial x}{\partial t}, \quad c\frac{\partial x}{\partial t} + \frac{\partial x}{\partial \nu} = 0. \tag{3.2}$$

We see immediately that $l = cv$, i.e. that the length of a cell is directly related to its speed. It also follows via careful use of the chain rule that

$$\left.\frac{\partial v}{\partial x}\right|_t = \frac{\partial v/\partial \nu}{\partial x/\partial \nu} = \frac{\partial^2 x/\partial \nu \partial t}{-l} = \frac{1}{l}\left.\frac{\partial l}{\partial t}\right|_\nu \approx \frac{\dot{L}_j}{L_j}. \tag{3.3}$$

Eq. (3.3) shows that the RER of individual cells is related to the spatial velocity gradient of the tissue, which can be measured from an image via $(\partial l/\partial x)|_t/c$. Call this $G(x)$, say (this was measured, for example, by [3]). Eq. (3.3) also shows how the velocity gradient can be written $\dot{F}F^{-1}$, where $F = \partial x/\partial \nu$ is a form of *deformation gradient*.

Noting that spatial hormone distributions (of auxin in particular) regulate cell expansion, we can model growth directly in a continuous framework using position-dependent functions of extensibility and yield, which we encompass in an RER distribution $G(x)$ (Fig. 3). We can integrate $\partial v/\partial x = G(x)$ to recover $v(x) = v_0 + \int_0^x G(x')\,\mathrm{d}x'$ and $l(x) = cv$, where $l_0 = cv_0$ is the length of cells where they enter the domain. $G(x)$ is a hump-like function [9], confined (by definition) to an elongation zone ($0 < x < \mathcal{L}$, say). Mature

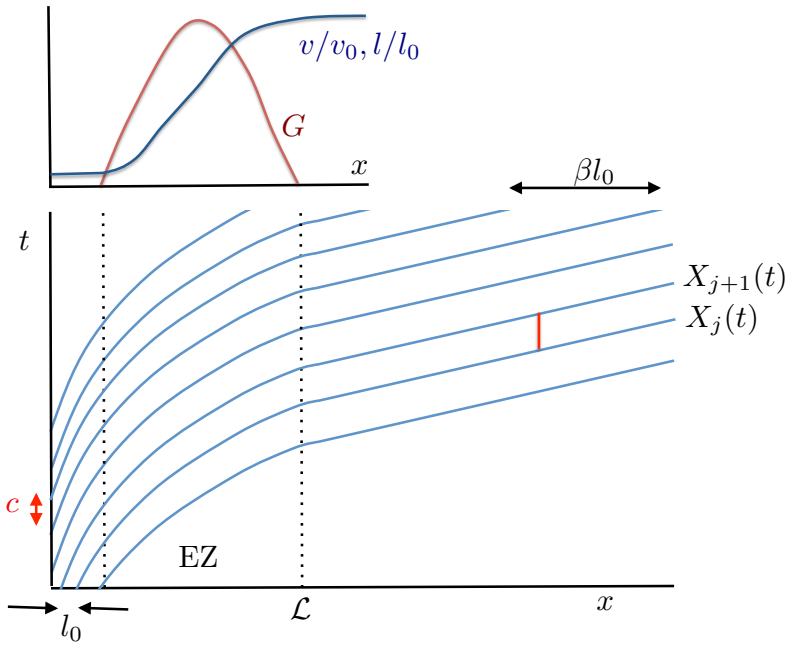

Figure 3: The elongation zone (EZ) along a root (between vertical dotted lines) is characterised by a region of positive RER, indicated by the function $G(x)$, where x measures distance from the meristem. Cells enter the EZ at length l_0, speed v_0 at rate c and leave with length βl_0 and speed βv_0, where the amplification factor β satisfies (3.4). The space-time diagram shows cell vertex locations $X_j(t)$. The vertical red line indicates how $X_j(t) = X_{j+1}(t + c)$.

cells leave the elongation zone with length βl_0 where

$$\beta = 1 + \frac{c}{l_0}\int_0^{\mathcal{L}} G(x')\,\mathrm{d}x'. \tag{3.4}$$

In a root, mature cells are stationary with respect to the surrounding soil, implying that the speed with which the root tip penetrates the soil is $\beta v_0 = \beta l_0/c$. In *Arabidopsis*, β can be as large as 30 [9].

Finally, the evolution of a scalar field $m(x,t)$ within individual cells satisfies

$$\left.\frac{\partial m}{\partial t}\right|_{\nu} = \left.\frac{\partial m}{\partial t}\right|_{x} + \left.\frac{\partial m}{\partial x}\right|_{\nu}\frac{\partial x}{\partial \nu} = \frac{\partial m}{\partial t} + v\frac{\partial m}{\partial x}, \tag{3.5}$$

which students of fluid mechanics will recognise as a *material* or *Lagrangian derivative*. This is equivalent to evaluating $\mathrm{d}m/\mathrm{d}t$ along the characteristic $\mathrm{d}x/\mathrm{d}t = v$. The cell vertex locations in Fig. 3 illustrate the characteristics. A little algebra shows that the cell density, $\rho = 1/l$, satisfies

$$\frac{\partial \rho}{\partial t} + \frac{\partial}{\partial x}(\rho v) = 0, \tag{3.6}$$

which is equivalent to the mass conservation equation for a compressible flow in one dimension. This demonstrates that the *cell flux* in the frame of the root tip is ρv (which is a constant, $1/c$ in the present simple example). In the presence of cell division, (3.6) would be supplemented by a source term on its right-hand-side.

3.2 Growth against an external load

As an illustration, working on the assumption that spatial hormone patterns regulate cell extensibility and yield, making $\phi = \phi(x)$ and $Y = Y(x)$ in (2.11), the steady cell length distribution can be calculated from

$$\frac{1}{c}\frac{\mathrm{d}l}{\mathrm{d}x} = \phi(x)\theta\left[\Pi - \Sigma - Y(x)/\theta\right]_+. \tag{3.7}$$

Here the term Σ has been added to represent the compressive stress that runs along a line of cells that are expanding against an axial load imposed at the tip of the organ (e.g. a primary root), neglecting other loads on the cells. A crude model of an elongation zone has $Y = Y_0$ in $0 < x < \mathcal{L}$ and $Y = Y_1$ in $x > \mathcal{L}$, where Y_0 is sufficiently small to allow growth but Y_1 is sufficiently large to suppress growth. Then, assuming cells grow from length l_0 at $x = 0$ to their mature length βl_0 at $x = \mathcal{L}$, where they move at speed v_∞ with respect to the meristem, it follows that

$$v_\infty = \frac{\beta l_0}{c} = v_0 + \theta\left[\Pi - \Sigma - \frac{Y_0}{\theta}\right]\Phi, \quad \text{where} \quad \Phi = \int_0^{\mathcal{L}} \phi(x)\,\mathrm{d}x. \tag{3.8}$$

Assuming mature cells are stationary with respect to their environment (soil or agar), then the meristem moves with speed v_∞ with respect to the environment. Eq. (3.8) illustrates how the speed of the root tip is determined by the collective expansion of all the cells in the EZ. If this motion induces a drag $\Sigma = kv_\infty$ for some $k > 0$, then

$$v_\infty = \frac{l_0/c + [\Pi\theta - Y_0]\,\Phi}{1 + \theta k \Phi}. \tag{3.9}$$

This expression illustrates how growth rates may be suppressed by an environmental drag k via passive mechanical resistance; the drag may also induce actively regulated changes of growth rate via *thigmotropic* or touch-sensitive responses.

4 Quasi-1D models for bending of slender tissues

Previously, we scaled up the stress/strain-rate relation for a cell wall (2.7) to a single cell (2.11), introducing the geometric parameter θ. Let us now repeat the exercise for multiple cells in a root cross-section (Fig. 4). We idealise it as a set of cell walls under tension containing cytoplasm under turgor pressure $P \equiv \Pi$. Integration of a force balance across the whole root cross section [24] (assuming no external load on the root) gives

$$P\mathcal{A} = \langle Y\rangle + \left\langle \frac{1}{\phi}\mathrm{RER}_{\mathrm{cell}}\right\rangle, \quad \text{for} \quad P\mathcal{A} > \langle Y\rangle, \tag{4.1}$$

balancing the total force due to turgor with the net tension induced in walls, modelled by (2.7). Here angle brackets denote integration along slender cell walls, accounting for variable wall thickness if necessary; in the single-cell example above, for example, $\langle Y\rangle$ was expressed as phY. $\mathcal{A}$ is the root cross-sectional area and turgor is assumed uniform across the root. Suppose all cells elongate at the same rate, i.e. with the same RER. Then

$$\mathrm{RER} = \frac{1}{\langle \phi^{-1}\rangle}(P\mathcal{A} - \langle Y\rangle), \quad \text{for} \quad P\mathcal{A} > \langle Y\rangle, \tag{4.2}$$

defining the effective extensibility $\langle \phi^{-1}\rangle^{-1}$ and yield $\langle Y\rangle$ of the cross-section. This is the Lockhart equation once more, now upscaled (or homogenized) for a complete root cross-section. An immediate consequence is that the peripheral (epidermal) cells have the greatest contribution to $\langle \phi^{-1}\rangle$ and $\langle Y\rangle$, by virtue of having the largest length of cell walls of all layers [24].

If material properties vary slightly across the root cross-section, then there may be a slight gradient in RER across the cross section, inducing bending of the root centreline. Let f measure perpendicular distance from a diameter across the root (Fig. 4), such that the diameter is parallel to the axis of curvature of the root. Then geometry (see box below) tells us that $\mathrm{RER}_{\mathrm{cell}} \approx \mathrm{RER} + \mathrm{CGR}f$, where curvature growth rate $\mathrm{CGR} = \mathrm{d}\kappa/\mathrm{d}t$ for a root segment. A *moment balance* across the cross-section, assuming no external couple on the root (multiply (4.1) by f and integrate over the cross-section, [24]) reveals that

$$-\left\langle \frac{f^2}{\phi}\right\rangle \mathrm{CGR} = \langle fY\rangle + \left\langle \frac{f}{\phi}\right\rangle \mathrm{RER} - P\int f\,\mathrm{d}A, \text{ for } P\mathrm{A} > \langle Y\rangle. \tag{4.3}$$

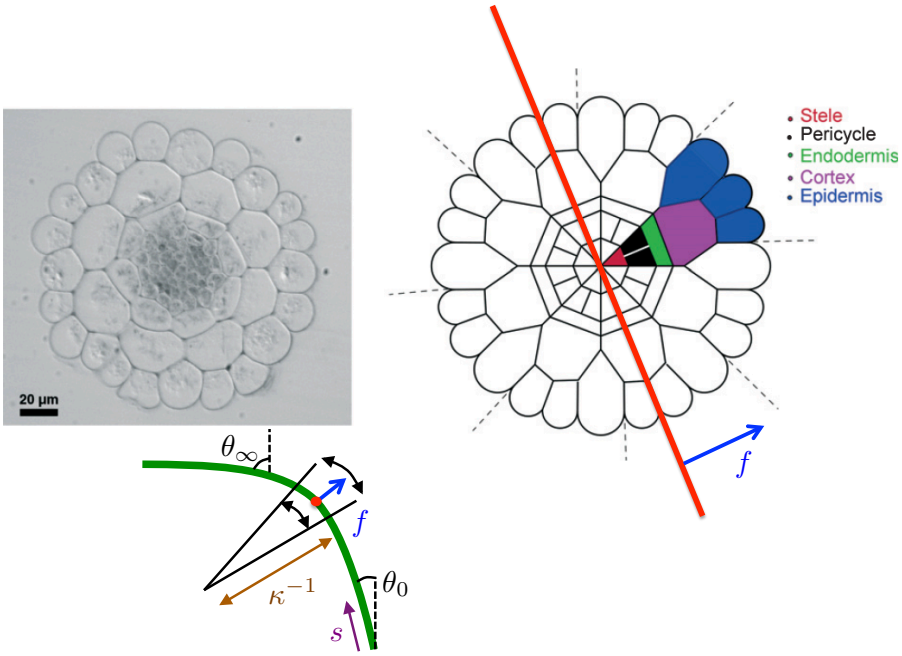

Figure 4: A cross-section of an *Arabidopsis* primary root (top, left) and an idealised representation of the five cell layers (right) (adapted from [24]). In a tropic response, material properties on one side of the root are altered with respect to the other, inducing bending of the root centreline by differential expansion. The red line indicates the axis around which the root bends and f measures perpendicular distance from this line. A transverse view of the root (bottom, left) shows how the elongation rate is greater on the outer bend ($f > 0$) than the inner bend ($f < 0$); κ^{-1} is the local radius of curvature.

This shows how asymmetries in yield, extensibility and turgor can each generate curvature of the structure.

A short segment of root, with centreline arclength δ_0 and curvature κ, subtends an angle ψ at its centre of curvature, a distance $1/\kappa$ from the centreline. Thus $\psi = \delta_0/(1/\kappa) = \kappa\delta_0$. The arclength δ through the segment a radial distance f from the centreline subtends the same angle ψ. Thus $\kappa\delta_0 = \delta/[(1/\kappa) + f]$ and so $\delta = \delta_0(1+\kappa f)$. Assuming δ_0 and κ are functions of time, and that $\kappa f \ll 1$, then $\dot{\delta}/\delta = \dot{\delta}_0/\delta_0 + \dot{\kappa} f$, i.e. $\mathrm{RER}_{\mathrm{cell}} = \mathrm{RER} + \mathrm{CGR} f$ for a cell a distance f from the centreline of the segment.

Equation (4.3) shows how transverse gradients in ϕ are amplified by stretching to induce bending. Considering this effect in isolation, we can write $\mathrm{d}\kappa/\mathrm{d}t = A_0\mathrm{RER}$ for the root segment, where A_0 characterises the material asymmetry in extensibility across the root. If the curvature remains sufficiently weak, we may define distance along the structure with arclength s instead of linear distance x, but still exploit the 1D model derived in §3. From (3.5), we may write the CGR as a material derivative, so that

$$\frac{\partial \kappa}{\partial t} + v\frac{\partial \kappa}{\partial s} = A_0 \frac{\mathrm{d}v}{\mathrm{d}s}, \tag{4.4}$$

showing how curvature of a root segment is amplified by stretching as it is swept through the elongation zone.

We can then write down a simple model of root gravitropism. Let θ_0 be the angle of the root tip to the vertical and θ_∞ the angle of root to the vertical at the top of the elongation zone (Fig. 4). Then $\theta_\infty = \theta_0 + \int_0^{\mathcal{L}} \kappa \, \mathrm{d}s$. Assuming mature cells are immobile with respect to their surroundings, that there are no external forces constraining lateral motions of the elongation zone, and that the gravitropic signal is communicated rapidly (by auxin transport) to tissues in comparison to the timescale for growth, then

a model for the gravitropic response of the root is

$$\frac{\partial \kappa}{\partial t} + v\frac{\partial \kappa}{\partial s} = \beta \frac{\mathrm{d}v}{\mathrm{d}s}\sin\left[\theta_\infty - \int_0^{\mathcal{L}} \kappa \,\mathrm{d}s\right], \quad \frac{\mathrm{d}\theta_\infty}{\mathrm{d}t} = -\kappa_\infty v_\infty \tag{4.5}$$

where (4.5) must be solved with $\kappa(0,t) = 0$ to determine $\kappa(\mathcal{L},t) \equiv \kappa_\infty$. Here β is a parameter that measures the degree of asymmetry induced by the gravitropic signal, arising from gravity sensing at the root tip. The path of the root tip with respect to the surroundings is determined by the evolution of θ_∞ as tissue is steadily extruded from the elongation zone at axial speed v_∞. The full dynamics of this model await investigation; the constraints of the environment on the root's motion are an important omission.

The simple model (4.5) is a variant of the famous 'sine law' model for shoot gravitropism, which takes the form $\partial\kappa/\partial t = -\beta\sin\theta - \gamma\kappa$, where $\kappa = \partial\theta/\partial s$ [6, 7]. The β term reflects the local response to the gravity stimulus that takes place in the shoot (the advective derivative has been neglected). The γ term models *proprioception*, an inherent tendency of the organ to straighten.

5 Constitutive models for 3D anisotropic growing materials

To generalise the simple constitutive models of §2 from one to three spatial dimensions, at either the cell or tissue level, we must reformulate them using tensor calculus. Let us first briefly review descriptions of materials that have linear constitutive laws. We write stress as the symmetric tensor $\boldsymbol{\sigma} = \boldsymbol{\sigma}^T$ (where T denotes transpose) such that the (vector) force per unit area acting on a surface with unit normal $\mathbf{n}$ is $\boldsymbol{\sigma}\cdot\mathbf{n}$. A small deformation $\mathbf{u}$ is characterised by strain $\mathsf{e} = \frac{1}{2}(\nabla\otimes\mathbf{u} + (\nabla\otimes\mathbf{u})^T)$. An *incompressible* material has $\nabla\cdot\mathbf{u} = \mathrm{tr}(\mathsf{e}) = 0$ (where tr denotes trace), implying that material elements do not change volume.

To clarify notation, vectors are represented as 3×1 column vectors with respect to Cartesian coordinates, and tensors as 3×3 matrices. ∇ is the spatial gradient operator, and can be written $(\partial/\partial x, \partial/\partial y, \partial/\partial z)^T$ or $(\partial/\partial x_1, \partial/\partial x_2, \partial/\partial x_3)^T$. The dot product of two vectors $\mathbf{a} = (a_1,a_2,a_3)^T$ and $\mathbf{b} = (b_1,b_2,b_3)^T$ is $\mathbf{a}\cdot\mathbf{b} = \mathbf{a}^T\mathbf{b} = a_1b_1 + a_2b_2 + a_3b_3$. Thus if $\mathbf{u} = (u_1,u_2,u_3)$, then $\nabla\cdot\mathbf{u} = \partial u_1/\partial x_1 + \partial u_2/\partial x_2 + \partial u_3/\partial x_3$. The *outer product* $\otimes$ is defined such that $\{\mathbf{a}\otimes\mathbf{b}\}_{ij} \equiv \{\mathbf{a}\mathbf{b}^T\}_{ij} = a_ib_j$ for i and j taking values 1, 2 and 3, and $(\mathbf{a}\otimes\mathbf{b})^T = (\mathbf{a}\mathbf{b}^T)^T = \mathbf{b}\mathbf{a}^T = \mathbf{b}\otimes\mathbf{a}$.

In linear elasticity, we assume a linear relation between stress and strain, of the form $\boldsymbol{\sigma} = \mathsf{C}:\mathsf{e}$, where C is a fourth order *stiffness tensor*. (In terms of components, $\sigma_{ij} = \sum_{k,l} C_{ijkl}e_{kl}$.) For a *homogeneous isotropic* material (a very poor description of plant tissues), C is characterised by just two parameters (despite having 81 components), the elastic *Lamé constants* λ and μ.

Using index notation, using symmetry and related arguments, it can be shown that

$$C_{ijkl} = \lambda\delta_{ij}\delta_{kl} + \mu(\delta_{ik}\delta_{jl} + \delta_{il}\delta_{jk}) \tag{5.1}$$

where $\delta_{ij} = 1$ if $i = j$ and 0 otherwise, giving $\boldsymbol{\sigma} = \lambda\mathsf{I}\,\mathrm{tr}(\mathsf{e}) + 2\mu\mathsf{e}$, where I is the second-order identity tensor. In the incompressible limit, $\lambda\to\infty$ and $\mathrm{tr}(\mathsf{e})\to0$ with their product remaining finite, in the form of a Lagrange multiplier ($-p$, a pressure). In this case, stress and strain are related in 3D by

$$\boldsymbol{\sigma} = -p\mathsf{I} + 2\mu\mathsf{e}, \tag{5.2}$$

with μ sometimes termed the *shear modulus*. To illustrate how this generalises the 1D model presented in §2.1, consider an incompressible rod undergoing uniaxial extension, with $\mathbf{u} = \alpha(z\hat{\mathbf{z}} - \frac{1}{2}x\hat{\mathbf{x}} - \frac{1}{2}y\hat{\mathbf{y}})$, so that $\mathsf{e} = \alpha(\hat{\mathbf{z}}\otimes\hat{\mathbf{z}} - \frac{1}{2}\hat{\mathbf{x}}\otimes\hat{\mathbf{x}} - \frac{1}{2}\hat{\mathbf{y}}\otimes\hat{\mathbf{y}})$. The transverse components of stress (in the x and y directions) vanish if $p = -\mu\alpha$, in which case the axial (z) component of stress is $3\mu\alpha$. Thus we recover the 1D description of linear elasticity, with a linear relation between axial stress and axial strain α, with coefficient $E = 3\mu$.

An incompressible isotropic viscous material with a linear stress/strain-rate relation (i.e. a Newtonian fluid) satisfies a relation analogous to that of an incompressible elastic material, namely $\boldsymbol{\sigma} = -p\mathsf{I} + 2\mu\dot{\mathsf{e}}$, where now μ is a viscosity and $\dot{\mathsf{e}}$ is a rate-of-strain tensor, defined in terms of the velocity field $\mathbf{v}$ as $\dot{\mathsf{e}} = \frac{1}{2}(\nabla \otimes \mathbf{v} + (\nabla \otimes \mathbf{v})^T)$ with $\nabla \cdot \mathbf{v} = 0$. Pressure p appears again as an isotropic component of the stress, ensuring incompressibility.

5.1 Anisotropy

The plant cell wall can be modelled as a composite *fibre-reinforced* material, having cellulose microfibrils embedded in a pectin matrix. The anisotropic structure of the cell wall, combined with the orientation of cell walls within a tissue, are crucial to the plant's ability to alter its shape in order to adapt to its environment. It is instructive to examine the form of the elastic stiffness tensor for a segment of cell wall, treating it as a thin sheet (so using a 2D approximation). Let $\mathbf{a}$ be a unit vector in the fibre direction, lying in the plane of the sheet, and assume all fibres are locally parallel (an over-simplification). The material is then considered to be *transversely isotropic*, requiring us to distinguish quantities aligned in the fibre direction ($\|$) from those in the perpendicular direction within the plane of the sheet ($\perp$).

Consider small deformations, for which the stress–strain relation remains linear (for more general nonlinear theory see [35]). We define the *structure tensor* $\mathsf{A} = \mathbf{a} \otimes \mathbf{a}$, the strain magnitude in the fibre direction $e_\| = \mathbf{a} \cdot \mathsf{e} \cdot \mathbf{a}$, and the strain in the fibre direction $\mathsf{e}_a = (\mathsf{e} \cdot \mathbf{a}) \otimes \mathbf{a} + \mathbf{a} \otimes (\mathsf{e} \cdot \mathbf{a})$. Then, in the incompressible limit, the stiffness tensor can be reduced (using symmetry and related arguments [57]) to

$$\boldsymbol{\sigma} = -p\mathsf{I} + \mu_2 e_\| \mathsf{A} + 2\mu_\perp (\mathsf{e} - \mathsf{e}_a) + 2\mu_s \mathsf{e}_a. \tag{5.3}$$

Thus in addition to the familiar stress components ($-p\mathsf{I} + 2\mu_\perp \mathsf{e}$) are additional contributions due to fibres, involving two additional material parameters. We can interpret the constants by examining the stress–strain relation in some special cases.

> In a 2D plane containing the fibre direction, a local basis is provided by orthogonal unit vectors $\mathbf{a}$ and $\mathbf{b}$ where $\mathbf{a} \cdot \mathbf{b} = 0$, $\mathbf{a} \cdot \mathbf{a} = 1$ and $\mathbf{b} \cdot \mathbf{b} = 1$. Consider a 2D deformation with strain $\mathsf{e} = \lambda(\mathbf{a} \otimes \mathbf{a} - \mathbf{b} \otimes \mathbf{b})$ for some constant λ, implying extension in the fibre direction and compression orthogonal to this (with no deformation in the direction normal to the wall, making this a *plane strain* approximation). Then $e_\| = \lambda$, $\mathsf{e}_a = \lambda \mathbf{a} \otimes \mathbf{a}$ is the tensile strain in the fibre direction, $\mathsf{e} - \mathsf{e}_a = -\lambda \mathbf{b} \otimes \mathbf{b}$ is the compressive strain orthogonal to the fibres, and $\boldsymbol{\sigma} = -p\mathsf{I} + (\mu_2 + 2\mu_s)\mathsf{e}_a + 2\mu_\perp(\mathsf{e} - \mathsf{e}_a)$. For this deformation, reading off the stresses in the $\|$ and $\perp$ directions, we see that the effective extensional stiffness in the fibre direction is $\mu_\| = \mu_s + \frac{1}{2}\mu_2$, while that perpendicular to the fibres is $\mu_\perp$. Likewise, a shear deformation, for which $\mathsf{e} = \gamma(\mathbf{a} \otimes \mathbf{b} + \mathbf{b} \otimes \mathbf{a})$ for some constant γ, has $\boldsymbol{\sigma} = -p\mathsf{I} + 2\mu_s \mathsf{e}$, identifying μ_s as an elastic shear modulus.

Typically, fibre-reinforced materials can be very stiff in the fibre direction, potentially restricting any stretching, so that $\mu_\| \gg \mu_\perp$. This is a key property exploited by plant cell walls to avoid radial expansion while allowing axial elongation. In the extreme limit, $\mu_2 \to \infty$ and $e_\| \to 0$ with their product remaining finite. We can introduce a Lagrange multiplier T representing a tension induced in the fibres, giving

$$\boldsymbol{\sigma} = -p\mathsf{I} + T\mathsf{A} + 2\mu_\perp(\mathsf{e} - \mathsf{e}_a) + 2\mu_s \mathsf{e}_a. \tag{5.4}$$

In this case, just two parameters, the matrix stiffness $\mu_\perp$ and shear stiffness μ_s, regulate the restricted motion, and the induced tension T ensures no stretching in the fibre direction.

> This approach has a direct analogue for anistropic fluid motion, for which μ_2, $\mu_\perp$ and μ_s instead have interpretations as viscosities [25]. Fluids have the advantage that a linear constitutive law can be used to describe large deformations, but then the fibres will deform with the fluid. They evolve according to
>
> $$\frac{\partial \boldsymbol{a}}{\partial t} + (\mathbf{v} \cdot \nabla)\,\mathbf{a} + \zeta \mathbf{a} = (\mathbf{a} \cdot \nabla)\,\mathbf{v} \tag{5.5}$$

where $\zeta = \frac{1}{2}\mathbf{a}\cdot(\nabla\otimes\mathbf{v}+(\nabla\otimes\mathbf{v})^T)\cdot\mathbf{a}$ is the component of the rate-of-strain tensor in the fibre direction. We recognise the first two terms as a material derivative; the remaining terms suppress stretching of $\mathbf{a}$ by the flow, ensuring that $\mathbf{a}\cdot\mathbf{a}=1$ throughout.

So far, we have described the effects of a population of aligned fibres. For a material with fibre orientations $\mathbf{a}(\Omega)$ having a distribution $\rho(\Omega)$ over *solid angle* Ω, the stiffness tensor can have an isotropic component of the form (5.1), plus an anisotropic component of the form

$$\mathsf{C}_f = Y_\mathrm{f}\int \mathsf{A}\otimes\mathsf{A}\,\rho(\Omega)\,\mathrm{d}\Omega \tag{5.6}$$

for some stiffness parameter Y_f. If the fibres lie in a plane, the integral is over the polar angle θ and six independent components of C_f can be derived [19, 50].

In a 2D computational model of individual cells in an elongated tissue, Fozard et al. [30] combined a finite element discretisation of an anisotropic linear constitutive law (5.3) for periclinal cells with a scalar Lockhart model for anticlinal cells, to mimic root bending.

5.2 Growth in 3 dimensions

Large deformations require a nonlinear elastic theory, which brings further technical complications, many of which are bypassed in the short account below. First, it is necessary to distinguish between a reference (Lagrangian) state and a deformed state, with deformations described by a mapping between them. From this one can define a *deformation gradient* F where $\mathrm{d}\mathbf{x}=\mathsf{F}\mathrm{d}\mathbf{X}$ or $F_{ij}=\partial x_i/\partial X_j$. Here $\mathbf{X}$ labels material points in the undeformed configuration and $\mathbf{x}(\mathbf{X},t)$ gives their location in the deformed state.

Within this framework, growth is described by considering two mappings: from the original state to an intermediate (grown) state; and from the grown state to the physical state, accounting for elastic deformations. This decomposition [52, 54], which appears also in the theory of nonlinear plasticity, has deformation gradient $\mathsf{F}=\mathsf{F}_e\mathsf{F}_g$. $\mathsf{F}_g(t)$ represents time-dependent growth at some time t and F_e the instantaneous elastic deformation that is required to accommodate an imposed load.

The velocity of a material particle is $\mathbf{v}=\dot{\mathbf{x}}$ (for fixed $\mathbf{X}$), so that the velocity gradient with respect to Lagrangian variables is $\partial\mathbf{v}/\partial\mathbf{X}=(\partial\mathbf{v}/\partial\mathbf{x})\mathsf{F}$ but also $\partial\dot{\mathbf{x}}/\partial\mathbf{X}=\dot{\mathsf{F}}$. Thus the velocity gradient with respect to Eulerian variables is $\dot{\mathsf{F}}\mathsf{F}^{-1}=\partial\mathbf{v}/\partial\mathbf{x}$, generalising (3.3). In terms of the composite deformation, $\dot{\mathsf{F}}\mathsf{F}^{-1}=\mathsf{F}_e\dot{\mathsf{F}}_g\mathsf{F}_g^{-1}\mathsf{F}_e^{-1}$. Here the F_e tensors are (in the jargon) *pushing forward* the velocity gradient in the intermediate state to the current state, so we can identify $\dot{\mathsf{F}}_g\mathsf{F}_g^{-1}$ as the velocity gradient of the unstressed grown state. This is taken as the analogue of $\dot{e}_g$ in (2.14).

We can now see how the Lockhart model (2.3, 2.4) can be formulated for 3D anistropic materials, although we will only touch on a few of the technical details, staying as close as possible to the simpler models we have seen so far. Here we follow [12] and [50]. Considering first purely elastic deformations, the *second Piola–Kirchoff stress* S_e and the *Lagrangian strain* $\mathsf{E}_e=\frac{1}{2}(\mathsf{F}_e^T\mathsf{F}_e-\mathsf{I})$ are related via a *strain energy function* $\mathcal{W}$ as $\mathsf{S}_e=\partial\mathcal{W}/\partial\mathsf{E}_e$. In general, $\mathcal{W}$ is a function of *strain invariants*, which may account for anisotropy. A simpler approach uses the *hyperelastic* Hookean model $\mathcal{W}=\frac{1}{2}\mathsf{E}_e:\mathsf{C}:\mathsf{E}_e$ where C is a 4th-order stiffness tensor that accommodates anisotropy, so that $\mathsf{S}_e=\mathsf{C}:\mathsf{E}_e$ and $\mathsf{C}=\partial^2\mathcal{W}/\partial^2\mathsf{E}_e$. This is generalised to incorporate growth using

$$\mathsf{E}_e=\mathsf{C}^{-1}:\mathsf{S}_e\quad \dot{\mathsf{F}}_g\mathsf{F}_g^{-1}=\gamma\left[\mathsf{E}_e-\mathsf{E}_Y\right]_+ \tag{5.7}$$

for some constant γ. In terms of the driving stress S_e, which depends on turgor, and yield stress S_0,

$$\dot{\mathsf{F}}_g\mathsf{F}_g^{-1}=\gamma\left[\mathsf{C}^{-1}:(\mathsf{S}_e-\mathsf{S}_0)\right]_+. \tag{5.8}$$

Here the threshold term $[\cdot]_+$ (a tensor ramp function [50]) is a simplified version of more complex plasticity approaches [12], such that for a tensor T decomposed into its eigenvalues λ_n and eigenvectors

$\mathbf{t}_n$ we have

$$\mathsf{T} = \sum_{n=1}^{d} \lambda_n \mathbf{t}_n \otimes \mathbf{t}_n \quad \text{and} \quad [\mathsf{T}]_+ = \sum_{n=1}^{d} \max(\lambda_n, 0)\, \mathbf{t}_n \otimes \mathbf{t}_n. \tag{5.9}$$

Note that in this model, a single stiffness tensor captures anisotropy both in the viscous creep (5.8) and in the elastic response (5.7).

Boudon et al. [12] have implemented this model by resolving individual cell walls in a tissue using a 3D finite-element discretisation. A similar framework was adopted in [13]. Models incoporating mechanical feedback on growth are reviewed in [1].

6 Discrete modelling approaches for multicellular tissues

A popular class of models resolve the structure of individual cells in an inherently discrete formulation. This approach can be computationally intensive but it avoids the requirement to average over cells in order to describe a tissue, thereby resolving features that may be lost in spatial averaging. Furthermore, there is the advantage that biochemical processes can be resolved in individual cells and coupled to mechanical processes [21, 38, 55]. The continuum models of §5 are of sufficient complexity to require solution by (typically) a finite-element method. There is a logic in identifying individual cells as natural "elements" in the spatial discretisation. One can either take a top-down approach, projecting the bulk (averaged) description down onto individual elements, or a bottom-up approach by defining the mechanical properties of each element directly. The two approaches may not always be consistent, as the top-down description requires fields to vary smoothly from cell to cell and may rest on *ad hoc* approximations that are not immediately related to properties at the cell scale.

Cell geometry can be represented in various ways. A popular grid-based model is the *Cellular Potts* scheme, where an individual cell is represented using sets of neighbouring elements on a fixed grid. Using a sufficiently fine grid, this method will resolve elaborate cell shapes, albeit at high computational cost. At a much coarser level, *cell-centre* models assign cells to a single spatial location and model cell-cell interactions. We focus here on intermediate **vertex-based** descriptions, where a 2D (3D) cell is treated as a polygon (polyhedron), allowing its shape to be defined economically by the location of its vertices. In 2D, a monolayer is represented as a tiling of the plane by polygons; in 3D, a tissue is defined by space-filling polyhedra. The polygons need not be regular or periodic. Growth and mechanics are simulated by deriving appropriate rules for the motion of the vertices. For plant cells, which typically have a cytoplasm dominated by a large vacuole at fixed turgor pressure, this is a natural approach as attention can be focused on the mechanically influential cell walls.

Vertex-based models differ in their choice of constitutive assumption. One popular model assigns to each cell a mechanical energy [27, 28, 46, 60], which can account for strain of individual cells and cell-cell adhesion. The arrangement of cells in space is then determined by allowing cell configurations to adjust until the global mechanical energy is minimized. Direct minimization identifies one or more equilibria (the system can be "glassy" with a rough energy landscape, with different minima accessed from different initial conditions). Alternatively a model for viscous dynamics is employed to track the unsteady evolution to an equilibrium. Growth is modelled through cell expansion (for example via a Lockhart-based model, e.g. [30]) or through cell division (requiring a model for cell cycling and division orientation, e.g. [34]).

6.1 The mechanical energy of a cell

Cell-based models typically rely on simple geometric invariants (the perimeter, surface area or volume of a cell), defined with respect to 'target' values of each at which the corresponding energy contribution is minimal. We illustrate this for a 2D layer of cells; generalisations to 3D follow naturally. The energy of a single cell (labelled by i) is often written [27, 46, 58]

$$U_i = \tfrac{1}{2}K_a(A_i - A_0)^2 + \tfrac{1}{2}K_l(L_i - L_0)^2, \tag{6.1}$$

where K_a and K_l are positive parameters. The first term describes the energy associated with the cell's area A_i (so that large K_a constrains A_i to remain close to a reference area A_0), and so is a measure of the stiffness of the cytoplasm. The second term characterises the energy associated with the cell's perimeter, and its deviation from a reference perimeter L_0. Separately, the contributions define a pressure and a tension for the cell defined by $\partial U_i/\partial A_i$ and $\partial U_i/\partial L_i$ respectively:

$$P_i = K_a(A_i - A_0), \quad T_i = K_l(L_i - L_0). \tag{6.2}$$

For a single cell, U_i might be minimized by a configuration in which $A_i < A_0$ and $L_i > L_0$, with the competition between bulk compression ($P_i < 0$) and peripheral tension ($T_i > 0$) giving the cell an intrinsic rigidity (via so-called 'tensegrity'). The energy of a tissue formed of confluent cells can then be written $U = \sum_i U_i$; additional terms might measure the strength of adhesion between particular cell types.

Growth can be accommodated by allowing for cell expansion (varying A_0 or L_0) or by explicitly modelling cell division. Conversely, the process of cell death and extrusion of an individual cell from the monolayer can also be described. Both division and extrusion change the topology of the monolayer, by introducing or removing cells. Cells may also undergo neighbour exchange (through a so-called *T1 transition*). This reorganisation of the tissue is a microscopic manifestation of plasticity. It is a common feature of developing animal tissues but less common in plants, where cells typically adhere tightly to their neighbours.

> The strain energy of an elastic continuum is normally defined in terms of *strain invariants*, measuring the deformation from a reference state, expressed in terms of eigenvalues of (say) the right Cauchy–Green tensor $\mathsf{F}^T\mathsf{F}$. For a growing elastic material, the elastic strains are measured relative to an evolving intermediate state. The vertex-based model uses a formulation that is more directly interpretable in terms of cellular quantities, namely cell area, cell perimeter and their target values.

Plant-specific variants of (6.1) include the following model for the superficial cells of the shoot apical meristem [34]:

$$U = \sum_{j\in\text{walls}} \frac{k_w}{2}\left(\frac{L_j - L_j^0}{L_w^0}\right)^2 - \sum_{i\in\text{cells}} \Pi_i A_i - \sum_{i\in\text{cells}} P_{i,\text{int}} V_{i,\text{ int}}\,. \tag{6.3}$$

The first term describes tensile forces in anticlinal walls; the second describes forces normal to anticlinal walls due to cell turgor pressure Π_i (assumed uniform in all cells in [34]); the third represents pressure from the underlying tissues, producing a force acting in the direction normal to the cell layer. Anistropy is introduced by making anticlinal wall stiffness k_w a function of orientation. Minimisation of U, by movement of cell vertices, brings the cell layer to equilibrium; slower cell growth was implemented in [34] using a Lockhart law

$$\frac{\mathrm{d}L_j^0}{\mathrm{d}t} = k_g\left(\frac{L_j - L_j^0}{L_j^0} - T_g\right)_+ \tag{6.4}$$

for some extensibility-like parameter k_g and a yield strain T_g. For now, we restrict attention to the simpler model (6.1). Related approaches include [16] (addressing turgor) and [42] (cell shape).

6.2 Cell topology and geometry

For large-scale discrete models, careful book-keeping is needed in order to keep track of relationships between vertices, cell edges, cell faces, and so on as a tissue evolves. Here we briefly outline one approach to address this, illustrating the approach in 2D.

An array of cells is defined in terms of a set of vertices (position vectors) $\mathbf{r}_k$, $k = 1, \ldots, N_v$, a set of *oriented edges* $\mathbf{t}_j$ (of length $l_j = |\mathbf{t}_j|$), $j = 1, \ldots, N_e$ and a set of *oriented cell faces* $\mathbf{a}_i$ (of area A_i), $1 = 1, \ldots, N_c$ (Figs 5 and 6). Here $\mathbf{r}_k$ and $\mathbf{t}_j$ are vectors in a 2D (x, y) plane, while $\mathbf{a}_i = A_i\boldsymbol{\epsilon}_i$ where $\boldsymbol{\epsilon}_i$ represents a rotation by $\pm\pi/2$, i.e. $\begin{pmatrix} 0 & \mp 1 \\ \pm 1 & 0 \end{pmatrix}$ in terms of Cartesian coordinates. Orientations of edges and faces are prescribed but arbitrary.

The *topology* of the monolayer (what connects with what) can be defined in terms of two *incidence matrices* [32] (Fig. 5). A, with elements A_{jk}, is an $N_e \times N_v$ matrix with elements 1 (or -1) when edge j is oriented

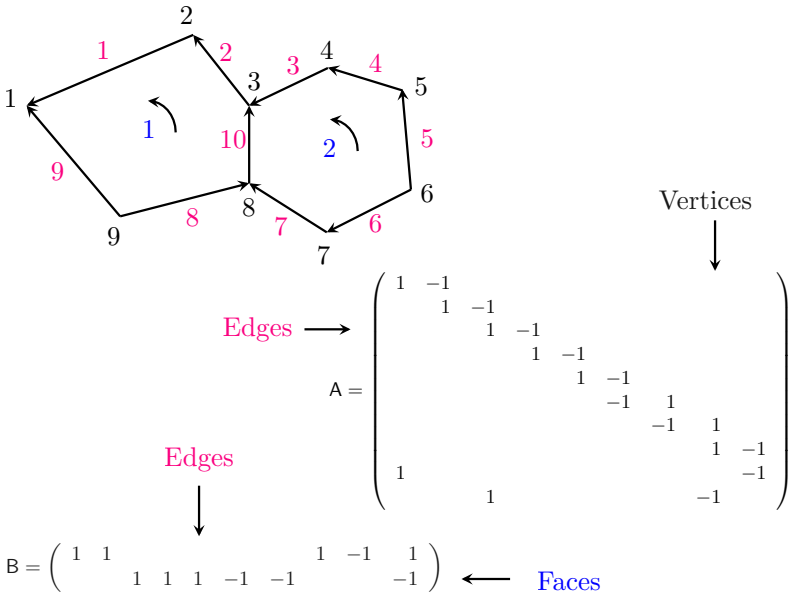

Figure 5: An illustration of the representation of cell topology through incidence matrices. Two cells, joined by a single edge, are defined by 9 vertices, 10 edges and 2 faces. The orientations of edges and faces are prescribed arbitrarily. The 10×9 matrix A shows which edges and vertices are connected (empty spaces are zeros), with 1 (-1) indicating an edge pointing into (out of) a vertex. The 2×10 matrix B shows which edges neighbour which face, and which are coherent with (1) or not coherent with (-1) the face.

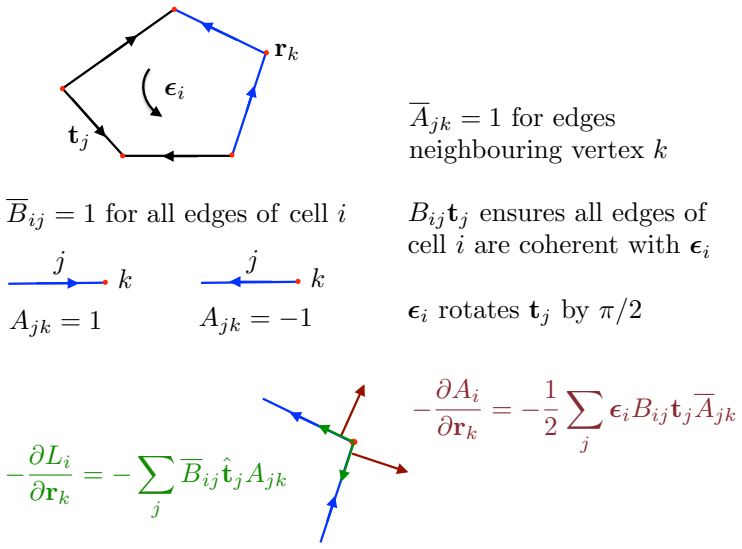

Figure 6: A schematic summarising the forces associated with area and perimeter changes in a vertex-based model.

into (or out of) vertex k, and zero otherwise. B, with elements B_{ij}, is an $N_c \times N_e$ matrix with elements ± 1 when edge j is on the boundary of cell i, taking values $+1$ if the edge is coherent with the orientation of the cell face and -1 if not; otherwise, all elements of B are zero. Replacing -1 with 1 in each matrix produces *adjacency matrices* $\overline{\mathsf{A}}$ and $\overline{\mathsf{B}}$, which identify neighbours but do not indicate orientation. The $N_c \times N_v$ matrix $\overline{\mathsf{C}} = \frac{1}{2}\overline{\mathsf{B}}\,\overline{\mathsf{A}}$ takes the value $\overline{C}_{ik} = 1$ if vertex k neighbours cell i, and is zero otherwise.

> A and B have interpretations as *discrete derivatives*, while A^T and B^T are *boundary operators*, identifying vertices bounding an edge or edges bounding a face. Since the edges of cells form closed loops, they have no boundary and so $\mathsf{A}^T\mathsf{B}^T = \mathsf{0}$ and $\mathsf{BA} = \mathsf{0}$.

The *geometry* of the monolayer (measuring its size) is defined by magnitudes of lengths and areas. Edges are defined by $\mathbf{t}_j = \sum_k A_{jk}\mathbf{r}_k$ (summing over all vertices), from which $l_j = \sqrt{\mathbf{t}_j \cdot \mathbf{t}_j}$ can be evaluated, along with the unit vector $\hat{\mathbf{t}}_j = \mathbf{t}_j/l_j$. The perimeter of cell i is then $L_i = \sum_j \overline{B}_{ij} l_j$ (summing over all edges). It follows that

$$\frac{\partial l_j}{\partial \mathbf{r}_k} = \hat{\mathbf{t}}_j A_{jk} \quad \text{and} \quad \frac{\partial L_i}{\partial \mathbf{r}_k} = \sum_j \overline{B}_{ij}\hat{\mathbf{t}}_j A_{jk}. \tag{6.5}$$

$-\partial L_i/\partial \mathbf{r}_k$ identifies two unit vectors aligned with edges of cell i where it meets vertex k, pointing out of the vertex (Fig. 6).

> To evaluate cell areas, integrate $\nabla \otimes \mathbf{x} = \mathsf{I}$ over cell i. Using the divergence theorem,
>
> $$A_i\mathsf{I} = \int_i \nabla \otimes \mathbf{x}\,\mathrm{d}A = \oint_{\partial i} \hat{\mathbf{n}} \otimes \mathbf{x}\,\mathrm{d}s = \sum_j \mathbf{n}_{ij} \otimes \mathbf{c}_j \equiv \sum_j \mathbf{n}_{ij}\mathbf{c}_j^T, \tag{6.6}$$
>
> where $\mathbf{n}_{ij} = -\boldsymbol{\epsilon} B_{ij}\mathbf{t}_j$ defines outward normals of cell i and $\mathbf{c}_j = \frac{1}{2}\sum_k \overline{A}_{jk}\mathbf{r}_k$ is the centroid of edge j. Noting that $\boldsymbol{\epsilon}_i^T = -\boldsymbol{\epsilon}_i$, $\boldsymbol{\epsilon}_i\boldsymbol{\epsilon}_i = -\mathsf{I}$ and that the tensor in (6.6) is symmetric, its transpose gives
>
> $$A_i\mathsf{I} = \sum_j \mathbf{c}_j \otimes \mathbf{n}_{ij} = \sum_j B_{ij}(\mathbf{c}_j \otimes \mathbf{t}_j)\boldsymbol{\epsilon}_i, \tag{6.7}$$
>
> so that $A_i\boldsymbol{\epsilon}_i = -\sum_j B_{ij}\mathbf{c}_j \otimes \mathbf{t}_j$. A further transpose gives $\mathbf{a}_i \equiv A_i\boldsymbol{\epsilon}_i = \sum_j B_{ij}\mathbf{t}_j \otimes \mathbf{c}_j$.

Some tedious algebra (e.g. [48]) reveals that

$$\frac{\partial A_i}{\partial \mathbf{r}_k} = \tfrac{1}{2}\sum_j \boldsymbol{\epsilon} B_{ij}\mathbf{t}_j\overline{A}_{jk} \equiv -\tfrac{1}{2}\sum_j \mathbf{n}_{ij}\overline{A}_{jk}. \tag{6.8}$$

$-\partial A_i/\partial \mathbf{r}_k$ identifies two outward normal vectors associated with the edges of vertex k bordering cell i (Fig. 6).

6.3 Vertex dynamics

Armed with (6.5) and (6.8), showing how the length and perimeter of cell i change when vertex k moves, we can now evaluate $\mathbf{f}_{ik} = \delta U_i/\delta \mathbf{r}_k$, the first variation of the energy of cell i with respect to a small displacement of vertex $\mathbf{r}_k$. This determines the elastic restoring force at $\mathbf{r}_k$ acting on cell i as

$$\mathbf{f}_{ik} = \sum_j \left[\tfrac{1}{2}P_i\boldsymbol{\epsilon} B_{ij}\mathbf{t}_j\overline{A}_{jk} + T_i\overline{B}_{ij}\hat{\mathbf{t}}_j A_{jk}\right]. \tag{6.9}$$

As Fig. 6 illustrates, the force at vertex k due to cell i has contributions from P_i acting along normals at the vertex, and from T_i acting along tangents. In equilibrium, the net force at vertex k and the net force on cell i must both vanish, i.e.

$$\sum_i \overline{C}_{ik}\mathbf{f}_{ik} = \mathbf{0}, \quad \sum_k \overline{C}_{ik}\mathbf{f}_{ik} = \mathbf{0}, \tag{6.10}$$

representing two *discrete divergences* of $\mathbf{f}_{ik}$.

A common model applies a drag η to each vertex, so that the equilibrium is reached by timestepping N_v coupled ODEs for $\mathbf{r}_k(t)$ of the form

$$\eta \frac{\mathrm{d}\mathbf{r}_k}{\mathrm{d}t} = -\sum_i \overline{C}_{ik}\mathbf{f}_{ik}. \tag{6.11}$$

This is the evolution equation (or rather, N_v ordinary differential equations) for vertex locations $\mathbf{r}_k$, coupled through the dependence of $\mathbf{f}_{ik}$ on $\mathbf{r}_k$ via A_i and L_i. An *initial condition* for cell vertices may come from an image, or may be constructed using a *Voronoi tessellation* of the plane. Suitable *boundary conditions* for the array of cells must also be chosen (a periodic box is a popular choice). Equation (6.11) is integrated until it reaches an equilibrium, satisfying (6.10a).

6.4 Cell and tissue stress

For a monolayer in equilibrium, evaluating $\sum_k \overline{C}_{ik}\mathbf{r}_k \otimes \mathbf{f}_{ik} \equiv A_i\boldsymbol{\sigma}_i$, where $\boldsymbol{\sigma}_i$ is the stress (force moment) associated with cell i, one finds after some algebra [36, 33, 48, 49] that

$$\boldsymbol{\sigma}_i = P_i\mathsf{I} + \frac{T_iL_i}{A_i}\mathsf{Q}_i, \quad \text{where} \quad \mathsf{Q}_i \equiv \frac{1}{L_i}\sum_j \overline{B}_{ij}l_j\hat{\mathbf{t}}_j \otimes \hat{\mathbf{t}}_j. \tag{6.12}$$

A simple way of interpreting these terms is to consider that under an imposed uniform strain E, A_i changes by $A_i\mathsf{I} : \mathsf{E} \equiv A_i\mathrm{tr}(\mathsf{E})$ and L_i changes by $L_i\mathsf{Q}_i : \mathsf{E}$ [49]. It turns out [48] that the principal axes of the cell stress tensor (more specifcally, of Q_i) align with those of the cell's shape tensor $\sum_k \overline{C}_{ik}\mathbf{r}_k \otimes \mathbf{r}_k$, showing that cell shape and cell stress are intimately coupled. The isotropic component of the stress in each cell $\frac{1}{2}\mathrm{tr}(\boldsymbol{\sigma}_i)$ reveals the *effective pressure* in each cell

$$P_{\mathrm{eff}} = P_i + \frac{T_iL_i}{2A_i} \tag{6.13}$$

with contributions from both the bulk and the periphery. For an isolated cell in equilibrium, with $P_{\mathrm{eff}} = 0$, we expect $P_i < 0$ (because $A_i < A_0$) and $T_i > 0$ (because $L_i > L_0$), the typical state of a turgid plant cell. For example a cell at fixed turgor, as in (6.3), has $P_i = -\Pi_i$.

The stress of the monolayer as a whole is

$$A\boldsymbol{\sigma} = \sum_i A_i\boldsymbol{\sigma}_i = \sum_i (P_iA_i\mathsf{I} + T_iL_i\mathsf{Q}_i). \tag{6.14}$$

These expressions for cell and tissue stress (6.12, 6.14) can be compared with, for example, (5.4), showing how the structure tensor for each cell wall $\hat{\mathbf{t}}_j \otimes \hat{\mathbf{t}}_j$ contributes additively to the total stress, resembling the structure tensor of fibres A.

Patterns of P_{eff} can show inherently discrete features (such as *force chains*) across cell monolayers [48]. The cell stress (6.12) and tissue stress (6.14) have been derived from an underlying energy (6.1), and sit outside a traditional continuum framework. However the tissue as a whole exhibits linearly elastic properties when perturbed from an equilibrium, and plastic properties if cell rearrangements take place.

Perturbing the monolayer about an equilibrium reveals its stiffness tensor as

$$\mathsf{C} = \frac{1}{A}\sum_i \left[K_aA_i^2\mathsf{I} \otimes \mathsf{I} + K_lL_i^2\mathsf{Q}_i \otimes \mathsf{Q}_i + L_iT_i(\mathsf{B}_i - \mathsf{Q}_i \otimes \mathsf{I})\right] \tag{6.15}$$

where B_i is a fourth-order tensor [49] defined in terms of $\mathbf{t}_j$ such that under strain E, the change in $L_i\mathsf{Q}_i$ is $L_i\mathsf{B} : \mathsf{E}$. This is the discrete analogue of (5.1) or (5.6). This expression shows explicitly how cell orientations can induce anisotropy in the tissue. The effective tissue bulk and shear moduli can be derived from C. If L_0 becomes so large that T_i becomes negative for some cells, then the cells lose resistance to shear (via an unjamming *phase transition* [10]). Tissue rigidity is promoted by inducing large tensions in cell walls. Notice that the tissue properties are recovered as sums, without requiring (for example) a periodicity assumption, commonly made when homogenizing cellular materials [45].

Further adaptions of the vertex model include hybridization with a centreline model of the kind described in §4 [29].

7 Plant cell wall mechanics and the origins of the Lockhart model

The primary plant cell wall is formed from an array of cellulose microfibrils, cross-linked by hemicellulose, embedded in a pectin matrix. Enzymes target distinct components: PME (pectin methylesterase) targets the matrix; XTH and expansin disrupt crosslinks; and so on. Microstructural models of the cell wall can be used to understand how enzyme action influences mechanical attributes such as yield stress or extensibility, and how the wall's architecture influences cell and tissue dynamics. Cellulose self-assembles in a synthase complex that migrates along cortical microtubules; thus the microtubules influence the wall's structure. The mechanosensitivity of microtubules and details of the wall's microstructure are very active areas of research [14, 17, 34, 43].

7.1 The matrix

We start with a very simple model of a growing cell wall as a thin viscous sheet, deriving the relation between the axial stress resultant T in terms of its strain rate, thickness h and viscosity μ.

Consider a sheet of initial length L_0, thickness h_0 that is subject to an extensional stretching flow of velocity magnitude U_0. For an incompressible Newtonian fluid, satisfying $\nabla\cdot\mathbf{v}=0$ and $\nabla\cdot\boldsymbol{\sigma}=\mathbf{0}$, where $\boldsymbol{\sigma}=-2+\mu(\nabla\otimes\mathbf{v}+\nabla\otimes\mathbf{v}^T)$ (see §5), the 2D Stokes equations are

$$\partial_x u+\partial_y v=0,\quad 0=-\partial_x p+\mu(\partial_x^2 u+\partial_y^2 u),\quad 0=-\partial_y p+\mu(\partial_x^2 v+\partial_y^2 v), \tag{7.1}$$

where the velocity field $\mathbf{v}=(u,v)$ is defined with respect to coordinates (x,y) and ∂_x is shorthand for $\partial/\partial x$. The components of the stress tensor are

$$\sigma_{xx}=-p+2\mu\partial_x u,\quad \sigma_{yy}=-p+2\mu\partial_y v,\quad \sigma_{xy}=\mu(\partial_y u+\partial_x v). \tag{7.2}$$

We assume the sheet is stress-free at its surfaces $y=0$ and $y=h$ (i.e. $\sigma_{xy}=\sigma_{yy}=0$ there).

Equations (7.1, 7.2) can be simplified by exploiting the sheet's slender geometry, using the small parameter $\epsilon\equiv h_0/L_0\ll 1$. Write $(x,y,h)=L_0(x^*,\epsilon y^*,\epsilon h^*)$, $(u,v)=U_0(u^*,\epsilon v^*)$, $(p,\boldsymbol{\sigma})=\mu(U_0/L_0)(p^*,\boldsymbol{\sigma}^*)$. Then in $0<y^*<h^*$, we re-write (7.1, 7.2) in terms of dimensionless variables as

$$\partial_{x^*}u^*+\partial_{y^*}v^*=0,\quad 0=-\partial_{x^*}p^*+\partial_{x^*}^2u^*+\epsilon^{-2}\partial_{y^*}^2u^*,\quad 0=-\partial_{y^*}p^*+\epsilon^2\partial_{x^*}^2v^*+\partial_{y^*}^2v^*, \tag{7.3}$$

with

$$\sigma_{xx}^*=-p^*+2\partial_{x^*}u^*,\quad \sigma_{yy}^*=-p^*+2\partial_{y^*}v^*,\quad \sigma_{xy}^*=\epsilon^{-1}\partial_{y^*}u^*+\epsilon\partial_{x^*}v^*. \tag{7.4}$$

Now expand all variables using $u^*=u_0^*+\epsilon^2u_1^*+\ldots$ etc. At leading order, $\partial_{y^*}^2u_0^*=0$; furthermore $\sigma_{xy}^*=0$ on $y^*=0$ and $y^*=h^*$ implies $\partial_{y^*}u_0^*=0$ there. Thus $u_0^*=u_0^*(x^*,t^*)$. $\partial_{y^*}v_0^*=-\partial_{x^*}u_0^*$ implies $v_0^*=-y^*\partial_{x^*}u_0^*$ (assuming $v_0^*=0$ on $y^*=0$). Thus $\partial_{y^*}^2v_0^*=0$, implying $\partial_{y^*}p_0^*=0$. $\sigma_{0yy}^*=0$ on $y^*=0$ and h^* implies $p_0^*=2\partial_{y^*}v_0^*=-2\partial_{x^*}u_0^*$, giving finally that $\sigma_{0xx}^*=4\partial_{x^*}u_0^*$.

Restoring this expression to dimensional units we obtain the stress/strain-rate relation $\sigma_{xx}=4\mu\partial_x u$, implying that the sheet has *extensional viscosity* 4μ.

The stress resultant $T=\sigma_{xx}h$ therefore satisfies $T=4\mu h\partial_x u$, so that the extensibility in (2.7) (at least, that part of it arising from stretching of the matrix) can be expressed in terms of wall thickness and viscosity as

$$\phi=1/(4\mu). \tag{7.5}$$

For a wall of spatially uniform thickness, the extensional flow of material in the wall (relative to a point on its outer surface) is $\mathbf{v}=(\alpha x,-\alpha y)$, where α is the RER. In the absence of sources of wall material, the wall thickness satisfies $\mathrm{d}h/\mathrm{d}t=-\alpha h$ (stretching induces thinning). In practice, we expect metabolic processes to be depositing material on the wall's inner surface at $y=h$ in order to maintain the wall's thickness during growth (Fig. 7).

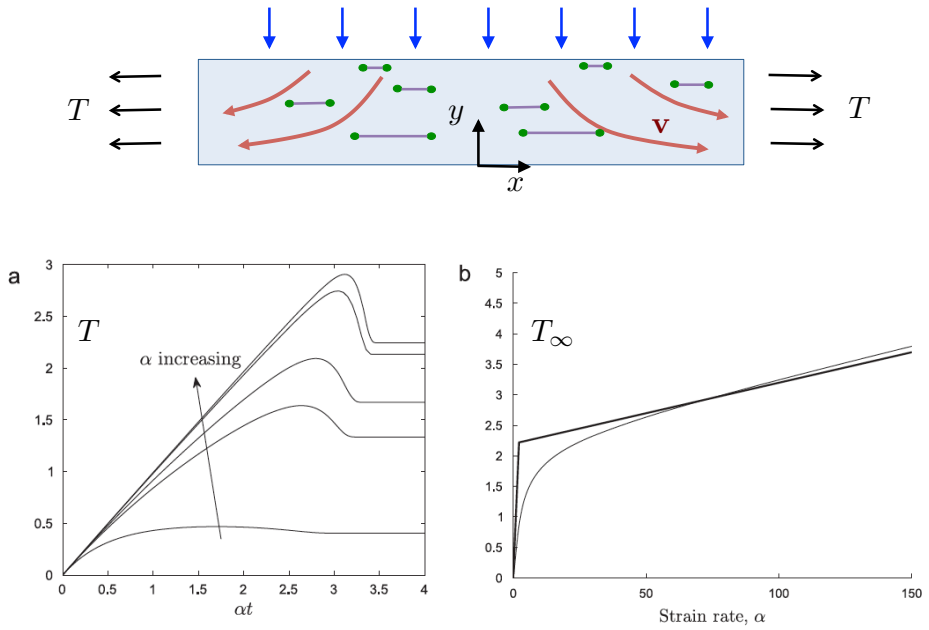

Figure 7: Top: a schematic of an element of wall undergoing stretching. At the inner surface, matrix, fibres and crosslinks are assembled and deposited (blue arrows). Fibres (green dots) are assumed to be normal to the page. Crosslinks (purple) are extended by the stretching of the wall, breaking before they reach the outer wall at $y = 0$. The wall elongates with velocity field $\mathbf{v} = \alpha(x, -y)$, where α is the RER. Bottom: (a) Stress resultant T versus strain, for different values of strain rate α; (b) large-time stress T_∞ versus strain rate, showing (thick line) a piecewise linear approximation to the smoother prediction of the model (7.7) (thin line); from [22].

7.2 Fibres, crosslinks and the origins of the Lockhart model

Now consider a cylindrical cell, elongating along its axis, with fibres oriented in the transverse direction. Suppose the fibres resist stretching, so that the strain-rate in the wall is $\dot{\mathbf{e}} = \alpha\hat{\mathbf{z}}\otimes\hat{\mathbf{z}} - \alpha\hat{\mathbf{r}}\otimes\hat{\mathbf{r}}$. Then the viscous analogue of (5.4) gives the stress field as $\boldsymbol{\sigma} = -p\mathsf{I} + T\hat{\boldsymbol{\theta}}\otimes\hat{\boldsymbol{\theta}} + 2\mu_\perp\dot{\mathbf{e}}$. In this simple example, the hoop stress $\sigma_{\theta\theta} = T$ that inhibits swelling decouples from the axial extension. In practice, fibres that are not exactly transverse will be rotated as the wall extends (via (5.5)), complicating the story [23]. For example, fibres deposited at a fixed angle at the inner wall will rotate towards the cell's axis as the wall stretches, while moving towards the outer wall; as they rotate, they suppress cell elongation. The cell's effective extensibility then depends on the fibre orientation integrated across the wall, which depends on the manner in which fibres were deposited at earlier times.

To examine the role of crosslinks, consider the simplest possible scenario, when fibrils are deposited transversely on the inner wall (perpendicular to the axis of the cell), with hemicellulose crosslinks formed between them. As the cell elongates, fibres migrate towards the outer wall of the cell, while being separated by the stretching of the wall (Fig. 7). The distance between fibres satisfies $\mathrm{d}L/\mathrm{d}t = \alpha L$ on $\mathrm{d}y/\mathrm{d}t = -\alpha y$, while the density of crosslinks between fibres $n(y,t)$ satisifes $\partial_t n - \alpha y\partial_y n = -k_{\mathrm{off}}n$, for some breakage rate k_{off}. We can model each crosslink as a spring with stiffness κ and unstressed length L_0. Taking an off-rate (breakage rate) of the form

$$k_{\mathrm{off}} = k_0 \exp\left(\beta^2 \frac{\kappa(L-L_0)^2}{2k_bT}\right), \tag{7.6}$$

where k_bT is a unit of thermal energy and $\beta \ll 1$ is a constant, then bonds break close to the outer wall where cross-links are sufficiently extended. (The kinetics depend here on a ratio of mechanical to thermal energy; other models [2] estimate the mechanical energy as a force times a distance, which is linear rather than quadratic in strain). We are here assuming that broken crosslinks cannot reform within the wall. The

stress resultant in the wall can be modified to incorporate the additional effect of crosslinks as

$$T = \int_0^h n(y,t)\kappa(L - L_0)\,\mathrm{d}y + 4\mu h\alpha. \tag{7.7}$$

This simple model can be used to determine the dependence of stress on the RER α. If RER is sufficiently small, cross-links break close the inner surface of the wall (they break before migrating very far). Increasing α carries crosslinks into the wall and extends them, increasing n and thus T. If RER is sufficiently large, crosslinks migrate close to the outer surface of the wall before breaking once very extended. This is a nearly saturated state, becoming insensitive to further increases in RER. The net effect is a nonlinear response between T and α (Fig. 7a,b), with characteristics of the plastic response in (2.2). For a strain increasing linearly in time at rate α, the model shows an initial elastic response (with stiffness $\mathcal{E} = n_0\kappa L_0 h$), a long-time viscous response characteristic of (2.3) [22]. The yield stress has magnitude $\mathcal{E}\log(1/\beta)$.

Significant work needs to be done to further develop microscale models of cell wall structure (such as the computational study of [61]), that incorporate relevant biochemistry and thermodynamics [4], and then scale these up to mechanical models of whole tissues, to understand how cell wall architecture influences plant morphology.

References

[1] O. Ali, V. Mirabet, C. Godin, and J. Traas. Physical models of plant development. *Annual review of cell and developmental biology*, 30:59–78, 2014.

[2] O. Ali and J. Traas. Force-driven polymerization and turgor-induced wall expansion. *Trends in plant science*, 21(5):398–409, 2016.

[3] L. R. Band, S. Úbeda-Tomás, R. J. Dyson, A. M. Middleton, T. C. Hodgman, M. R. Owen, O. E. Jensen, M. J. Bennett, and J. R. King. Growth-induced hormone dilution can explain the dynamics of plant root cell elongation. *Proc. Nat. Acad. Sci.*, 109(19):7577–7582, 2012.

[4] A. Barbacci, M. Lahaye, and V. Magnenet. Another brick in the cell wall: biosynthesis dependent growth model. *PLoS One*, 8(9):e74400, 2013.

[5] T. I. Baskin and O. E. Jensen. On the role of stress anisotropy in the growth of stems. *J. Exp. Bot.*, 64(15):4697–4707, 2013.

[6] R. Bastien, T. Bohr, B. Moulia, and S. Douady. Unifying model of shoot gravitropism reveals proprioception as a central feature of posture control in plants. *Proc. Nat. Acad. Sci.*, 110(2):755–760, 2013.

[7] R. Bastien, S. Douady, and B. Moulia. A unified model of shoot tropism in plants: photo-, gravi-and propio-ception. *PLoS computational biology*, 11(2):e1004037, 2015.

[8] L. Beauzamy, M. Louveaux, O. Hamant, and A. Boudaoud. Mechanically, the shoot apical meristem of arabidopsis behaves like a shell inflated by a pressure of about 1 mpa. *Front. Plant Sci.*, 6:1038, 2015.

[9] G. T. Beemster and T. I. Baskin. Analysis of cell division and elongation underlying the developmental acceleration of root growth in arabidopsis thaliana. *Plant Physiol.*, 116(4):1515–1526, 1998.

[10] D. Bi, J. Lopez, J. Schwarz, and M. L. Manning. A density-independent rigidity transition in biological tissues. *Nature Phys.*, 2015.

[11] D. Bonn, M. M. Denn, L. Berthier, T. Divoux, and S. Manneville. Yield stress materials in soft condensed matter. *Rev. Mod. Phys.*, 89(3):035005, 2017.

[12] F. Boudon, J. Chopard, O. Ali, B. Gilles, O. Hamant, A. Boudaoud, J. Traas, and C. Godin. A computational framework for 3d mechanical modeling of plant morphogenesis with cellular resolution. *PLoS Comp. Biol.*, 11(1):e1003950, 2015.

[13] B. Bozorg, P. Krupinski, and S. H. Jönsson. A continuous growth model for plant tissue. *Phys. Biol.*, 13:065002, 2016.

[14] S. A. Braybrook and H. Jönsson. Shifting foundations: the mechanical cell wall and development. *Curr. Op. Plant Biol.*, 29:115–120, 2016.

[15] I. Cheddadi, M. Genard, N. Bertin, and C. Godin. Coupling water fluxes with cell wall mechanics in a multicellular model of plant development. *PLOS Computational Biology*, 15(6):e1007121, 2019.

[16] F. Corson, O. Hamant, S. Bohn, J. Traas, A. Boudaoud, and Y. Couder. Turning a plant tissue into a living cell froth through isotropic growth. *Proc. Nat. Acad. Sci.*, 106(21):8453–8458, 2009.

[17] D. J. Cosgrove. Plant cell wall extensibility: connecting plant cell growth with cell wall structure, mechanics, and the action of wall-modifying enzymes. *J. Expt. Bot.*, 67(2):463–476, 2015.

[18] D. J. Cosgrove. Diffuse growth of plant cell walls. *Plant Physiol.*, 176(1):16–27, 2018.

[19] H. Cox. The elasticity and strength of paper and other fibrous materials. *Br. J. Appl. Phys.*, 3(3):72, 1952.

[20] E. De Langre. Effects of wind on plants. *Annu. Rev. Fluid Mech.*, 40:141–168, 2008.

[21] L. Dupuy, J. Mackenzie, T. Rudge, and J. Haseloff. A system for modelling cell–cell interactions during plant morphogenesis. *Ann. Bot.*, 101(8):1255–1265, 2007.

[22] R. Dyson, L. Band, and O. Jensen. A model of crosslink kinetics in the expanding plant cell wall: yield stress and enzyme action. *J Theor. Biol.*, 307:125–136, 2012.

[23] R. Dyson and O. Jensen. A fibre-reinforced fluid model of anisotropic plant cell growth. *J. Fluid Mech.*, 655:472–503, 2010.

[24] R. J. Dyson, G. Vizcay-Barrena, L. R. Band, A. N. Fernandes, A. P. French, J. A. Fozard, T. C. Hodgman, K. Kenobi, T. P. Pridmore, M. Stout, et al. Mechanical modelling quantifies the functional importance of outer tissue layers during root elongation and bending. *New Phytologist*, 202(4):1212–1222, 2014.

[25] J. Ericksen. Transversely isotropic fluids. *Colloid & Polymer Science*, 173(2):117–122, 1960.

[26] M. Fakih, J.-Y. Delenne, F. Radjai, and T. Fourcaud. Root growth and force chains in a granular soil. *Phys. Rev. E*, 99(4):042903, 2019.

[27] R. Farhadifar, J.-C. Röper, B. Aigouy, S. Eaton, and F. Jülicher. The influence of cell mechanics, cell-cell interactions, and proliferation on epithelial packing. *Curr. Biol.*, 17:2095–2104, 2007.

[28] A. G. Fletcher, M. Osterfield, R. E. Baker, and S. Y. Shvartsman. Vertex models of epithelial morphogenesis. *Biophys. J.*, 106:2291–2304, 2014.

[29] J. A. Fozard, M. J. Bennett, J. R. King, and O. E. Jensen. Hybrid vertex-midline modelling of elongated plant organs. *Interface Focus*, 6(5):20160043, 2016.

[30] J. A. Fozard, M. Lucas, J. R. King, and O. E. Jensen. Vertex-element models for anisotropic growth of elongated plant organs. *Front. Plant Sci.*, 4:233, 2013.

[31] A. Goriely. *The mathematics and mechanics of biological growth*, volume 45. Springer, 2017.

[32] L. J. Grady and J. R. Polimeni. *Discrete calculus: Applied analysis on graphs for computational science*. Springer Science & Business Media, 2010.

[33] B. Guirao, S. U. Rigaud, F. Bosveld, A. Bailles, J. Lopez-Gay, S. Ishihara, K. Sugimura, F. Graner, and Y. Bellaïche. Unified quantitative characterization of epithelial tissue development. *Elife*, 4:e08519, 2015.

[34] O. Hamant, M. G. Heisler, H. Jönsson, P. Krupinski, M. Uyttewaal, P. Bokov, F. Corson, P. Sahlin, A. Boudaoud, E. M. Meyerowitz, et al. Developmental patterning by mechanical signals in arabidopsis. *Science*, 322(5908):1650–1655, 2008.

[35] G. A. Holzapfel, R. W. Ogden, and S. Sherifova. On fibre dispersion modelling of soft biological tissues: a review. *Proc. Roy. Soc. A*, 475(2224):20180736, 2019.

[36] S. Ishihara and K. Sugimura. Bayesian inference of force dynamics during morphogenesis. *J. Theor. Biol.*, 313:201–211, 2012.

[37] O. E. Jensen and J. A. Fozard. Multiscale models in the biomechanics of plant growth. *Physiology*, 30(2):159–166, 2015.

[38] H. Jönsson, M. G. Heisler, B. E. Shapiro, E. M. Meyerowitz, and E. Mjolsness. An auxin-driven polarized transport model for phyllotaxis. *Proc. Nat. Acad. Sci.*, 103(5):1633–1638, 2006.

[39] D. Kierzkowski, N. Nakayama, A.-L. Routier-Kierzkowska, A. Weber, E. Bayer, M. Schorderet, D. Reinhardt, C. Kuhlemeier, and R. S. Smith. Elastic domains regulate growth and organogenesis in the plant shoot apical meristem. *Science*, 335(6072):1096–1099, 2012.

[40] D. Kierzkowski and A.-L. Routier-Kierzkowska. Cellular basis of growth in plants: geometry matters. *Curr. Opinion Plant Biol.*, 47:56–63, 2019.

[41] J. A. Lockhart. An analysis of irreversible plant cell elongation. *J. Theor. Biol.*, 8(2):264–275, 1965.

[42] R. M. Merks, M. Guravage, D. Inzé, and G. T. Beemster. Virtualleaf: an open-source framework for cell-based modeling of plant tissue growth and development. *Plant Physiol.*, 155(2):656–666, 2011.

[43] V. Mirabet, P. Das, A. Boudaoud, and O. Hamant. The role of mechanical forces in plant morphogenesis. *Ann. Rev. Plant Biol.*, 62:365–385, 2011.

[44] B. Moulia and M. Fournier. The power and control of gravitropic movements in plants: a biomechanical and systems biology view. *J. Exp. Bot.*, 60(2):461–486, 2009.

[45] N. Murisic, V. Hakim, I. Kevrekidis, S. Shvartsman, and B. Audoly. From discrete to continuum models of three-dimensional deformations in epithelial sheets. *Biophys. J.*, 109:154 – 163, 2015.

[46] T. Nagai and H. Honda. A dynamic cell model for the formation of epithelial tissues. *Phil. Mag. B*, 81:699–719, 2001.

[47] M. Nelson, L. Band, R. Dyson, T. Lessinnes, D. Wells, C. Yang, N. Everitt, O. Jensen, and Z. Wilson. A biomechanical model of anther opening reveals the roles of dehydration and secondary thickening. *New Phytologist*, 196(4):1030–1037, 2012.

[48] A. Nestor-Bergmann, G. Goddard, S. Woolner, and O. Jensen. A vertex-based model relating cell shape and mechanical stress in an epithelium. *Math. Med. Biol.*, 35:1–27, 2018.

[49] A. Nestor-Bergmann, E. Johns, S. Woolner, and O. E. Jensen. Mechanical characterization of disordered and anisotropic cellular monolayers. *Phys. Rev. E*, 97:052409, May 2018.

[50] H. Oliveri, J. Traas, C. Godin, and O. Ali. Regulation of plant cell wall stiffness by mechanical stress: a mesoscale physical model. *J. Math. Biol.*, 78(3):625–653, 2019.

[51] C. Prior, J. Moussou, B. Chakrabarti, O. E. Jensen, and A. Juel. Ribbon curling via stress relaxation in thin polymer films. *Proc. Nat. Acad. Sci.*, 113(7):1719–1724, 2016.

[52] E. K. Rodriguez, A. Hoger, and A. D. McCulloch. Stress-dependent finite growth in soft elastic tissues. *J. Biomech.*, 27(4):455–467, 1994.

[53] W. K. Silk and R. O. Erickson. Kinematics of plant growth. *J. Theor. Biol.*, 76(4):481–501, 1979.

[54] R. Skalak, G. Dasgupta, M. Moss, E. Otten, P. Dullemeijer, and H. Vilmann. Analytical description of growth. *J. Theor. Biol.*, 94(3):555–577, 1982.

[55] R. S. Smith, S. Guyomarc'h, T. Mandel, D. Reinhardt, C. Kuhlemeier, and P. Prusinkiewicz. A plausible model of phyllotaxis. *Proc. Nat. Acad. Sci.*, 103(5):1301–1306, 2006.

[56] E. Smithers, J. Luo, and R. Dyson. Mathematical principles and models of plant growth mechanics: from cell wall dynamics to tissue morphogenesis. *J. Exp. Bot.*, 2019.

[57] A. J. M. Spencer. *Deformations of fibre-reinforced materials.* Oxford University Press, 1972.

[58] D. B. Staple, R. Farhadifar, J. C. Roeper, B. Aigouy, S. Eaton, and F. Jülicher. Mechanics and remodelling of cell packings in epithelia. *Eur. Phys. J. E*, 33:117–127, 2010.

[59] R. Vandiver and A. Goriely. Tissue tension and axial growth of cylindrical structures in plants and elastic tissues. *Europhys. Lett,*, 84(5):58004, 2008.

[60] M. Weliky and G. Oster. The mechanical basis of cell rearrangement. i. epithelial morphogenesis during fundulus epiboly. *Development*, 109(2):373–386, 1990.

[61] H. Yi and V. M. Puri. Architecture-based multiscale computational modeling of plant cell wall mechanics to examine the hydrogen-bonding hypothesis of the cell wall network structure model. *Plant physiology*, 160(3):1281–1292, 2012.